Journal of Econometrics 214 (2020) 256–273

Contents lists available at ScienceDirect

Journal of Econometrics

journal homepage: www.elsevier.com/locate/jeconom

Econometric modelling of climate systems: The equivalence of energy balance models and cointegrated vector autoregressions

Felix Pretis *

Department of Economics, University of Victoria, BC, Canada
Nuffield College & INET at the Oxford Martin School, University of Oxford, UK

ARTICLE INFO

Article history:
Available online 27 May 2019

JEL classification:
C32
Q54

Keywords:
Cointegration
Vector autoregression
Climate
Energy balance
Indicator saturation

ABSTRACT

Estimates of both the human impact on climate as well as the economic impacts of climate change are crucial to inform policy decisions. Econometric modelling allows us to quantify these impacts and their uncertainties, but models have to be consistent with the underlying physics and the time series properties of the data. Here I show that energy-balance models of climate are equivalent to an econometric cointegrated system and can be estimated in discrete time. This equivalence provides a basis for the use of cointegration methods to estimate climate responses and test their feedback. Further, it is possible to use the estimated parameters to quantify uncertainties in integrated assessment models of the economic impacts of climate change. In an application I estimate a system of temperatures, ocean heat content, and radiative forcing including greenhouse gases, and find statistical support for the cointegrated energy balance model. Accounting for structural breaks from volcanic eruptions highlights large parameter uncertainties and shows that previous empirical estimates of the temperature response to increased CO_2 concentrations may be misleadingly low due to model-misspecification.

1. Introduction

Climate change is one of the greatest economic challenges facing humanity with potentially large costs from either action or inaction to tackle human-induced (anthropogenic) emissions. Informed policy decisions on climate change rely on both estimates of the magnitudes and uncertainties of the climate response to anthropogenic activity, as well as the climate-driven economic impacts. To quantify the uncertainties in responses and link econometric models with empirical climate models requires modelling approaches that are consistent with the underlying physics and the time series properties of the data. In this paper, I show that a two-component energy-balance model (EBM) of global mean climate is equivalent to an econometric cointegrated system, providing a physical basis for econometric methods that estimate climate responses and test feedback. Formally, I demonstrate the mathematical equivalence of a two-component energy balance model to a cointegrated system with parameter restrictions that can be mapped to a cointegrated vector autoregression (CVAR) and estimated in discrete time.

The motivation for a link between cointegrated econometric systems and energy balance models is two-fold. First, existing projections of economic impacts of climate change have not considered uncertainties around important parameters. The economic impacts of climate change derived from integrated assessment models (IAMs) such as FUND

* Correspondence to: Department of Economics, University of Victoria, BC, Canada.
E-mail address: fpretis@uvic.ca.

https://doi.org/10.1016/j.jeconom.2019.05.013
0304-4076/

(Waldhoff et al., 2011), PAGE (Hope, 2011; Hope et al., 1993), and DICE (Nordhaus, 2014) rely on simple energy balance models to model climate internally. However, uncertainties about the values of physical parameters in IAMs beyond the equilibrium climate sensitivity (ECS – the temperature response to a doubling in CO_2 concentrations) are conventionally not taken into account.[1] These uncertainties can have large impacts on the projected economic impacts of climate change, because the physical differences in climate models within IAMs already imply a range of economic damages from 5%–30% of future output (Calel and Stainforth, 2016). In particular, parameters are often assumed to be constant over time, and covariances across parameters (such as the ECS and the amount of energy it takes to increase temperatures) are often imposed without a statistical or physical basis. In contrast, a system approach to estimating EBMs based on CVARs can provide empirical parameter estimates and quantify their uncertainties which can subsequently guide economic impact projections.

Second, current climate-econometric research has generally not considered bi-directional feedback between the climate and the economy. Econometric studies beyond IAMs are split into two strands: one side empirically models the impact of climate on the economy, taking climate variation as given (e.g. Burke et al., 2015; Carleton and Hsiang, 2016; Dell et al., 2012, 2014; Pretis et al., 2018b), the other side models the impact of anthropogenic (e.g., economic) activity onto the climate by taking radiative forcing – the incoming energy from emitted radiatively active gases such as CO_2 – as given (e.g. Estrada et al., 2013; Hendry and Pretis, 2013; Kaufmann et al., 2011, 2013; Magnus et al., 2011; Storelvmo et al., 2016). This split in the literature is a concern as each strand considers conditional models, while feedback between the economy and climate likely run in both directions. By definition, both of these approaches cannot be correct at the same time. Most likely, neither is entirely correct; economic and environmental systems are typically determined with interdependencies in both directions. To test the presence and estimate the magnitude of these dependencies requires a framework that allows economic systems – well approximated by VARs (or panel VARs) – to be joined with empirical climate models consistent with the underlying physics.[2] In this paper, I take a first step in this direction and show that a two-component physics-based EBM can be mapped to a CVAR allowing adjustments and feedback to be estimated.

Estimation and inference on EBM model parameters in a system is not straightforward because climate observations are predominantly non-stationary time series, often with small numbers of observations (Estrada and Perron, 2014; Kaufmann et al., 2013; Kaufmann and Stern, 2002; Pretis and Hendry, 2013; Stern and Kaufmann, 2000). Econometric cointegration analysis can be used to overcome the inferential difficulties resulting from stochastic trends when that is the only source of non-stationarity, and is applied to test whether there exist combinations of non-stationary variables that are themselves stationary (see Hendry and Juselius 2001 for an overview, Schmith et al. (2012) for an application to sea level and temperature data, and Juselius (2011) as well as Kaufmann and Juselius (2013) for paleo-climate analyses). Inference in small samples can be improved through recent developments in bootstrap tests in cointegrated models (Cavaliere et al., 2012, 2015). In the present paper I establish the mathematical equivalence between CVARs and EBMs. Doing so provides a physical science basis for system cointegration, allowing EBMs to be estimated as a system and used to quantify parameter uncertainties within integrated assessment models. Further, the equivalence places the entire CVAR toolkit at the disposal of climate-econometric modelling.

In an application, I estimate a two-component EBM through the use of a CVAR and test it against the observational record. I find that tests against the statistical properties implied by the EBM do not reject the cointegrated model. Specifically, results from both standard cointegration tests as well as tests based on bootstrapping show that time series capturing global mean climate (surface temperatures, ocean heat content, and radiative forcing) form stationary relations and cointegrate in ways consistent with the underlying theory. Using indicator saturation methods (Hendry et al., 2008; Castle et al., 2015) I detect breaks and outliers in the estimated models which highlights the importance of accurately modelling sudden changes in forcing — ranging from volcanic to policy origins. Particularly, my results show that previous empirical estimates of the temperature response to increasing CO_2 concentrations (and parameter uncertainties in general) may be misleadingly low due to model mis-specification, partly induced by break-like volcanic aerosol forcing. My model estimates highlight the considerable uncertainty about parameters used in IAMs (such as the ocean heat capacity) which has not been accounted for in existing economic impact projections.

The paper is structured as follows: Section 2 introduces the two-component energy balance model, Section 3 shows the equivalence of the EBM and a cointegrated system. Section 4 demonstrates how the continuous-time EBM can be mapped to a discrete-time CVAR and estimated. Section 5 presents the application to a global mean climate system. Section 6 concludes.

2. Energy balance models (EBMs)

Energy balance climate models describe the change in temperatures as a function of incoming and outgoing radiation, with the simplest models approximating climate through global mean surface temperatures and aggregate radiative

[1] Nordhaus (2016) considers parameter uncertainties in DICE on the ECS and the carbon cycle, but not on the heat capacity of the atmosphere or ocean.

[2] Pretis (2017) discusses the validity of such conditioning and the split in climate econometrics, highlighting the importance of modelling the economic and climate sides jointly as a system. This allows us to test whether the magnitudes of feedback and adjustments are small enough to warrant a conditional analysis in either direction.

forcing. They are used within IAMs to model the climate response to different forcings from natural and anthropogenic sources (such as greenhouse gas emissions). Two-component physical energy-balance models (EBMs, see Gregory et al., 2002; Held et al., 2010; Pretis and Allen, 2013; Schwartz, 2012) extend the simple model to include ocean and atmosphere interactions and have tracked global mean climate well while remaining analytically tractable, but are rarely formally tested as estimation is difficult due to the non-stationarity of observations and multiple-equation nature of the system.

Two-component energy balance models of climate are characterised by a mixed upper layer (the shallow ocean/atmosphere) with low heat capacity and a deeper ocean layer with higher heat capacity, where heat capacity denotes the amount of energy needed to change the temperature of the component. The mixed upper component (denoted by subscript m) responds more quickly to perturbations (radiative forcing such as an increase in greenhouse gases[3]) and refers to the mixed layers of the atmosphere and shallow ocean. The deeper (denoted by subscript d) component responds slower and allows for delayed, recalcitrant warming (Held et al., 2010). In other words, if external forcing stopped and the system was in disequilibrium, high temperatures in the deep component would lead to a slow warming of the mixed atmosphere component (and vice versa).

A simple two-component EBM is given here as differential equations in (1)–(2) and explicitly takes ocean-atmosphere interactions into account. Let T_m be the temperature anomaly (deviations from a long-term mean in observed measurements) for the mixed layer, C_m is the component heat capacity and F denotes radiative forcing. Net heat flux denoting the net incoming energy is given by $Q = F - \lambda T_m$ where climate feedback is defined as λ, the change in downward net flux with temperatures T_m. The term λT_m captures the increasing outgoing long-wave radiation with increased temperatures. The upper component of the model describes the changes in heat content relative to the steady state $C_m \frac{dT_m}{dt}$ as a function of net flux $F - \lambda T_m$ and the heat exchange H with the lower component:

$$C_m \frac{dT_m}{dt} = -\lambda T_m + F - H. \tag{1}$$

The change in temperatures of the lower component $C_d \frac{dT_d}{dt}$ is given by:

$$C_d \frac{dT_d}{dt} = H, \tag{2}$$

where C_d denotes the effective heat capacity of the deep compartment and T_d is the associated temperature anomaly. The heat exchange between the bottom and upper component is assumed to be proportional to the difference in temperatures:

$$H = \gamma(T_m - T_d) \tag{3}$$

Substituting this expression into the above equations yields the two-component model as a system of two differential equations:

$$C_m \frac{dT_m}{dt} = -\lambda T_m + F - \gamma(T_m - T_d) \tag{4}$$

$$C_d \frac{dT_d}{dt} = \gamma(T_m - T_d). \tag{5}$$

Parameters $\lambda, \gamma, C_m, C_d$ are usually calibrated based on theory or general circulation model (GCM) simulations, or estimated using individual equations only. The economic impact models FUND (Waldhoff et al., 2011) and PAGE (Hope, 2011; Hope et al., 1993) use a single-equation calibrated energy balance model (without explicit representation of ocean-atmosphere interactions) as in Eq. (4) setting $\gamma = 0$, while DICE (Nordhaus, 2014) uses a calibrated two-component energy balance model as outlined here in the system of Eqs. (4) and (5). The feedback parameter λ is of particular interest as it determines the equilibrium response of surface temperatures T_m to a change in the forcing F (e.g. from increased CO_2 concentrations). In the following section I show that this system of differential equations is mathematically equivalent to a cointegrated system which can thus be estimated using econometric methods address the inherent non-stationarity from stochastic trends.

3. The equivalence of EBMs and cointegrated systems

Econometric cointegration analysis can be used to overcome difficulties associated with stochastic trends in time series and applied to test whether there exist combinations of non-stationary series that are themselves stationary. Here I show that the system of differential equations of the two-component EBM is equivalent to a cointegrated system with restrictions on the parameters, providing a physical interpretation of cointegration in this climate system. While there is a debate in the econometric literature on whether climate time series contain stochastic trends (suggesting a cointegration

[3] Together with many other factors (e.g. solar irradiance, reflective aerosols from volcanic eruptions, soot, etc.) the effect of GHGs is quantified through the concept of radiative forcing. In simple terms, this captures the change in energy in the atmosphere due to a change in concentration of a GHG or other factor. The radiative forcing effect, measured in watts per square metre (W m^{-2}), is calculated for the different forcing agents (e.g. GHGs, aerosols) and links the effect of the concentration of a gas on to temperatures.

treatment, see Kaufmann et al., 2010), or are better modelled through linear trends with breaks (e.g. Estrada et al., 2010), the analysis here concentrates on the cointegration approach.[4] The energy balance model in (4) and (5) can be expressed as

$$\frac{dT_m}{dt} = \frac{1}{C_m}\left[-\lambda T_m + F\right] - \frac{\gamma}{C_m}\left[T_m - T_d\right] \tag{6}$$

$$\frac{dT_d}{dt} = \frac{\gamma}{C_d}\left[T_m - T_d\right] \tag{7}$$

with no explicit formulation given for the changes in radiative forcing $\frac{dF}{dt}$ in the EBM. Let α and β denote $(p \times r)$ matrices (where $p = 3, r = 2$) corresponding to:

$$\alpha = \begin{pmatrix} \frac{1}{C_m} & -\frac{\gamma}{C_m} \\ 0 & \frac{\gamma}{C_d} \\ 0 & 0 \end{pmatrix} \text{ and } \beta' = (\beta_1, \beta_2)' = \begin{pmatrix} -\lambda & 0 & 1 \\ 1 & -1 & 0 \end{pmatrix}. \tag{8}$$

Then the two-component EBM in (6) and (7) can be written as the following system:

$$d\mathbf{Y} = \alpha\beta'\mathbf{Y}dt \tag{9}$$

where $\mathbf{Y} = (T_m, T_d, F)'$, a $(3 \times 1$ vector), with F assumed not adjust to $\mathbf{Y}$. It then holds that $\beta'\mathbf{Y}$ describes the long-run equilibrium relationships between the variables in the system, and the elements of α describe how the individual variables adjust to this long-run relation. Assuming stochastic processes (e.g. due to imperfect measurement and omitted variables) the two-component EBM can be written with a noise term $\mathbf{v}$ as an Ornstein–Uhlenbeck process given by the stochastic differential equation:

$$d\mathbf{Y} = \Pi\mathbf{Y}dt + \mathbf{dv} \tag{10}$$

$$= \alpha\beta'\mathbf{Y}dt + \mathbf{dv} \tag{11}$$

where Π is a $(p \times p)$ matrix of reduced rank $r = 2$ such that $\Pi = \alpha\beta'$. The noise term $\mathbf{dv} = DdW$ captures omitted effects from the model, with D being a $(p \times p)$ matrix and W a p-dimensional Brownian motion. Using the results in Kessler and Rahbek (2004, 2001), the formulation of the stochastic two-component energy balance model then implies that, if the continuous Ornstein–Uhlenbeck process is integrated[5] of order one, I(1), the series in the EBM cointegrate into two stationary relations given by $\beta'\mathbf{Y}$ with adjustment coefficients of α. The rank of the matrix Π determines the number of long-run relations, which is equal to two in the theory EBM. The physical stochastic two-component energy balance model is equivalent to a cointegrated system with parameter restrictions in continuous time in (12) and (13) where the expressions in brackets correspond to the cointegrating vectors, and the coefficients outside the brackets are the α adjustment coefficients in the cointegration model:

$$\frac{dT_m}{dt} = \underbrace{\frac{1}{C_m}}_{\alpha_{1,1}} \underbrace{\left[-\lambda T_m + F\right]}_{\beta_1'\mathbf{Y}} + \underbrace{\frac{\gamma}{C_m}}_{\alpha_{1,2}} \underbrace{\left[T_m - T_d\right]}_{\beta_2'\mathbf{Y}} + v_1 \tag{12}$$

$$\frac{dT_d}{dt} = \underbrace{\frac{\gamma}{C_d}}_{\alpha_{2,2}} \underbrace{\left[T_m - T_d\right]}_{\beta_2'\mathbf{Y}} + v_2. \tag{13}$$

The energy balance model implies that the three variables of upper component temperatures, lower component temperatures, and radiative forcing cointegrate into two stationary relations. The first, $\left(\beta_1'\mathbf{Y} = -\lambda T_m + F\right)$, a relation linking upper component temperatures to radiative forcing describing the net heat flux (Q). The second, $\left(\beta_2'\mathbf{Y} = T_m - T_d\right)$, a relation describing the heat transfer between the upper and lower component. In the EBM, upper component temperatures adjust to both cointegrating vectors, lower component temperatures adjust to the second cointegrating vector ($\alpha_{2,1} = 0$), and radiative forcing does not adjust to either cointegrating vectors ($\alpha_{3,1} = \alpha_{3,2} = 0$). With respect to the physical structure between variables, this implies that any stochastic trends present in the radiative forcing (where the stochastic component is driven by anthropogenic emission of greenhouse gases from stochastic economic activity) will be imparted onto the temperatures of the upper component, through which it transfers onto the lower component. Cointegration between these variables is a testable property, and cointegration analysis can further be used to estimate the EBM as a system and conduct inference on the parameters α and β for a given set of observations approximated by the model.

[4] Linking energy balance models to econometric models could equally be done using trend-stationary methods — see e.g. Estrada et al. (2013).

[5] In general a series that is $I(1)$, or integrated of order one needs to be differenced once to be stationary, while an I(2) series requires to be differenced twice.

4. Mapping of EBMs to CVARs and estimation as a system

The differential equations (12) and (13) describe the two-component energy balance model in continuous time, while observations are sampled at discrete intervals. I consider two approaches through which the EBM can be tested and estimated as a CVAR using discrete observations. First, Section 4.1.1 follows the literature on estimating continuous-time differential equations using VARs (see e.g. Phillips, 1991 and Kessler and Rahbek, 2004).[6] Second, an alternative is to interpret the EBM as a discrete time model (see e.g. Kaufmann et al., 2013 for a single-equation EBM), I consider this approach in Section 4.1.2. The difference between these two approaches in practise is small, and primarily affects the mapping of the adjustment coefficients α as the following sections show.[7]

4.1. Inference in the cointegrated continuous-time EBM using discrete-time observations

Discrete observations $\mathbf{Y}_t = \left(T_{m,t}, T_{d,t}, F_t\right)'$ of $\mathbf{Y} = (T_m, T_d, F)'$ can be written as a vector-autoregressive (VAR) process in Eq. (14):

$$\mathbf{Y}_t = \mathbf{A}\mathbf{Y}_{t-1} + \epsilon_{\mathbf{t}} \tag{14}$$

where the error term ϵ_t is assumed to be stationary. Let $\mathbf{P} = \mathbf{A} - I$, then (14) can be written in equilibrium correction form as a CVAR:

$$\Delta\mathbf{Y}_t = \mathbf{P}\mathbf{Y}_t + \epsilon_t \tag{15}$$

where Δ is the first difference operator, such that $\Delta Y_t = Y_t - Y_{t-1}$. The CVAR describes changes in the endogenous $\mathbf{Y}_t$ variables as a function of past changes in the long run-dynamics as captured through the coefficient matrix $\mathbf{P}$.

4.1.1. Exact solution to Ornstein Uhlenbeck process

In the exact solution of the Ornstein–Uhlenbeck process, the matrix $\mathbf{A}$ in the VAR in (14) equals the matrix exponential of the coefficient matrix in the continuous time EBM (11), $\mathbf{A} = \exp(\Pi)$, where $\Pi = \alpha\beta'$ and the error ϵ_t is given by $\epsilon_t \sim \mathrm{N}(0, \Sigma)$ — see supplementary material. There is then a direct mapping of the EBM parameters from Eq. (11) to the parameters in the discrete-time model (15). In particular, the coefficient matrix $\mathbf{P}$ in the CVAR relates to the EBM parameters α, β as:

$$\mathbf{P} = \mathbf{A} - I = \exp(\Pi) - I = \exp\left(\alpha\beta'\right) - I = \alpha\kappa\beta' = \tilde{\alpha}\beta' \tag{16}$$

where $\tilde{\alpha} = \alpha\kappa$ and the $(r \times r)$ matrix $\kappa = \left(\beta'\alpha\right)^{-1}\left[\exp\left(\beta'\alpha\right) - I\right]$, see supplementary material for a proof. This mapping implies that the two-component continuous-time EBM can be tested and estimated using a CVAR estimated on discrete observations: the rank of the coefficient matrix of the discrete-time VAR model equals that of the EBM, $\mathrm{rank}(\mathbf{P}) = \mathrm{rank}(\Pi) = \mathrm{rank}(\alpha\beta')$, and the matrix $\widehat{\mathbf{P}} = \hat{\tilde{\alpha}}\hat{\beta}'$ yields estimates of the EBM parameters given by β'. However, there is no one-to-one relation between the adjustment coefficients α in the EBM and the discrete-time CVAR parameters since $\tilde{\alpha} = \alpha\kappa$. This is intuitive as adjustment in the EBM may take place at a higher frequency than the sampling interval in discrete time. Even if α was identified in the continuous parameter model, it cannot be recovered from $\tilde{\alpha}$. Thus, restrictions in α are not directly preserved in the CVAR formulation. One exception on restrictions linking α and $\tilde{\alpha}$ occurs under weak-exogeneity for β. The forcing series is assumed to be weakly-exogenous for β (not adjusting to the cointegrating relations) in the EBM, thus $\alpha_{3,1} = \alpha_{3,2} = 0$. Given $\tilde{\alpha} = \alpha\kappa$ this implies that $\tilde{\alpha}_{3,1} = \tilde{\alpha}_{3,2} = 0$, forcing should also be weakly exogenous for β in the CVAR formulation.

The cointegrating vectors and adjustment coefficients are linked to the continuous-time two-component EBM such that upper component temperatures and radiative forcing enter the first cointegrating relation, $\beta_{1,1} = -\lambda, \beta_{1,2} = 0, \beta_{1,3} = 1$; upper component temperatures and lower component temperatures enter the second cointegrating relation $\beta_{2,1} = -\beta_{2,2} = 1$, and $\beta_{2,3} = 0$; and forcing is assumed to adjust to neither cointegrating relation $\tilde{\alpha}_{3,1} = \tilde{\alpha}_{3,2} = 0$. In matrix notation this can be expressed as:

$$\begin{aligned}\begin{pmatrix}\Delta T_{m,t}\\ \Delta T_{d,t}\\ \Delta F_t\end{pmatrix} &= \begin{pmatrix}\tilde{\alpha}_{1,1}\\ \tilde{\alpha}_{2,1}\\ 0\end{pmatrix}\begin{pmatrix}-\lambda & 0 & 1\end{pmatrix}\begin{pmatrix}T_{m,t-1}\\ T_{d,t-1}\\ F_{t-1}\end{pmatrix}\\ &+ \begin{pmatrix}\tilde{\alpha}_{1,2}\\ \tilde{\alpha}_{2,2}\\ 0\end{pmatrix}\begin{pmatrix}1 & -1 & 0\end{pmatrix}\begin{pmatrix}T_{m,t-1}\\ T_{d,t-1}\\ F_{t-1}\end{pmatrix} + \epsilon_t.\end{aligned} \tag{17}$$

This yields the discrete-time CVAR representation of the stochastic energy balance model and can be estimated and tested by estimating the CVAR in (15). The flexible nature of the CVAR also straight-forwardly allow extensions to EBMs with more than two-components, and potentially spatial dimensions through cointegrated spatial panel models.

---

[6] In particular, Theorem 1 in Kessler and Rahbek (2004).

[7] It is worth noting that the discretisation method moving from discrete to continuous time can have effects on the auto-correlation structure of the error term, and thus affect the statistical properties of the estimates (Sargan, 1974). Thus, while the solution to the OU process may imply a single lag, the time series properties of the observed variables may suggest a longer lag length.

4.1.2. Discrete-time approximation

An alternative approach to link EBMs and CVARs is to rely on a simple first-order Euler–Maruyama discrete time approximation (see e.g. Kloeden and Platen, 1992; Hutzenthaler et al., 2011; Calel and Stainforth, 2016) using $\frac{dT_m}{dt} \approx \Delta T_{m,t} = T_{m,t} - T_{m,t-1}$ and $\frac{dT_d}{dt} \approx \Delta T_{d,t} = T_{d,t} - T_{d,t-1}$. The system in (6) and (7) is then approximated as:

$$\Delta T_{m,t} = \frac{1}{C_m}\left[-\lambda T_{m,t-1} + F_{t-1}\right] - \frac{\gamma}{C_m}\left[T_{m,t-1} - T_{d,t-1}\right] + u_{1,t} \tag{18}$$

and

$$\Delta T_{d,t} = \frac{\gamma}{C_d}\left[T_{m,t-1} - T_{d,t-1}\right] + u_{2,t} \tag{19}$$

where $u_{1,t}$, $u_{2,t}$ denote stationary error terms. This system of equations is equivalent to a CVAR with restricted parameters where the expressions in brackets correspond to the cointegrating vectors, and the coefficients outside the brackets are the α adjustment coefficients in the cointegration model. The cointegrating vectors and adjustment coefficients are linked through the approximation to the EBM parameters such that: $\alpha_{1,1} = 1/C_m$, $\alpha_{2,1} = \alpha_{3,1} = 0$, $\beta_{1,1} = -\lambda$, $\beta_{1,2} = 0$, $\beta_{1,3} = 1$ further $\alpha_{2,2} = \gamma/C_d$, $\alpha_{1,2} = -\gamma/C_m$, $\alpha_{3,2} = 0$, $\beta_{2,1} = 1 = -\beta_{2,2}$ and $\beta_{2,3} = 0$. Cointegration is preserved in this CVAR formulation, the coefficient matrix $\mathbf{P}$ in the CVAR is interpreted as $\alpha\beta'$ in the EBM. Testing the rank and estimating the long-run relations given by β is identical to the results in 4.1.1. This generalises the results in Kaufmann et al. (2013) to the two-component EBM. The main difference to Section 4.1.1 lies in the interpretation of the adjustment coefficients α which map to the EBM parameters in this discrete-time approximation.

4.2. Testable properties implied by the EBM-CVAR mapping

The translation of a two-component EBM and a CVAR provides restrictions and properties which can be tested against observations. The rank of $\mathbf{P}$ determines the presence of long-run stationary relations, where the EBM with two components suggests the existence of two cointegrating vectors (rank of $\mathbf{P} = 2$). Conversely, if the rank of $\mathbf{P} = 0$, the series are integrated but do not cointegrate. The matrix $\mathbf{P}$ will have full rank if the series tested are in-fact stationary ($\sim$ I(0)) or if all endogenous stochastic trends can be explained by exogenous variables entering the cointegrating relation in a partial system. The number of cointegrating relations is chosen using the trace statistic which tests the null hypothesis that there are $r-1$ cointegrating relations against the null hypothesis that there are r relations (Johansen, 1988, 1995). To alleviate concerns associated with small samples, Bartlett corrections can be applied (Johansen, 2000) or a bootstrapping procedure to test the cointegrating rank (see Cavaliere et al., 2012) can be used. Using a system approach Johansen (1988) avoids many problems associated with single equation cointegration procedures (e.g. Engle and Granger, 1987) and does not require pre-testing of the individual series for stationarity (for a discussion of potential hazards see Pretis and Hendry, 2013). Formally the EBM implies the following testable properties of the estimated CVAR in Eq. (15):

1. Assessment of the model validity in view of the data, and determination of the appropriate lag-length (e.g. using Nielsen, 2006).
2. rank(Π) = rank($\mathbf{P}$) = 2 (Trace test e.g. using Johansen, 1988 or Cavaliere et al., 2012): the time series cointegrate to two stationary relations, linking upper component temperatures with radiative forcing, and lower component temperatures with upper component temperatures.
3. Restrictions in (17) on β are not rejected (likelihood ratio or bootstrap tests), estimates are statistically different from zero and theory-consistent.
4. Restrictions in (17) on $\tilde{\alpha}$ are not rejected, and estimates are statistically different from zero, (likelihood ratio or bootstrap tests) and theory-consistent.

Notably, estimating a two-component EBM through a CVAR avoids potential hazards associated with statistical and econometric climate models. The Johansen cointegration procedure requires no pre-testing of individual series for the order integration (up to I(1)) and takes the system nature of the model into account.

The CVAR modelling approach provides a foundation for coupling empirical EBMs with models of the macroeconomy by expanding the system in (15) using an explicit formulation for the forcing series F_t (e.g. endogenously modelling forcing along the lines of Hendry and Pretis, 2013). The forcing can be disaggregated into natural and anthropogenic factors, where concentrations of greenhouse gases are modelled as the accumulation of emissions driven by economic activity and social changes. Feedback of climate variables onto economic variables can then be estimated in the CVAR formulation yielding estimates of damages and the social cost of carbon. Further, the CVAR formulation of an EBM yields parameter estimates to assess the impacts of uncertainties in IAMs, and permits large-scale simulated climate models (e.g. GCMs) to be studied by estimating simple approximations to them using simulated model output and the CVAR approach together with the econometric time-series toolkit.

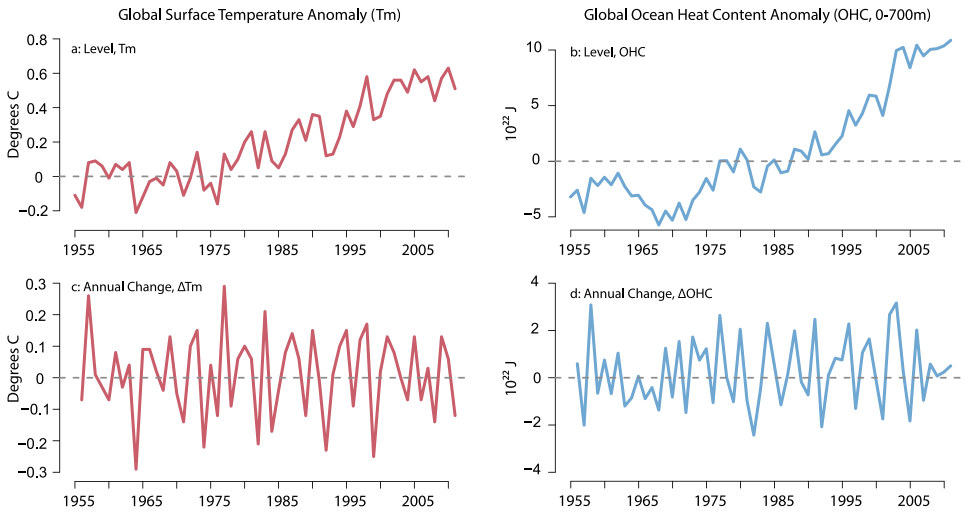

Fig. 1. Left: Global mean surface temperature anomaly in levels (panel *a*, top) and first differences (panel *c*, bottom). Right: Global ocean heat content anomaly from 0–700 m in levels (panel *b*, top) and first differences (panel *d*, bottom).

5. Application

To illustrate the mapping of the two-component EBM to a CVAR with restricted parameters, I estimate a CVAR using global-mean climate time series. The main results presented here do not place additional restrictions on the α adjustment coefficients and so follow the exact Ornstein–Uhlenbeck continuous-to-discrete time approach outlined in Section 4.1.1. The results for interpreting the EBM model in discrete time (placing additional restrictions on α) are reported in the supplementary material. Models are estimated using *PcGive* (Doornik and Hendry, 2013) and *CATS* in *Ox* (Doornik, 2016). Indicator saturation for break detection is implemented using the R-package *gets* (Pretis et al., 2018a) and *PcGive*.

5.1. Data

The upper/mixed component is specified as the atmosphere at the surface and temperatures are taken as global mean surface temperature anomalies from the GISS dataset (Hansen et al., 2010). Temperature anomalies are defined relative to the 1951–1981 temperature mean. The lower component is proxied by the ocean heat content (OHC) anomalies from 0–700 m (Levitus et al., 2009). This is a rough approximation as it omits the deep ocean and will therefore provide a high estimate of the adjustment speed of this component.[8] The series are graphed in Fig. 1. Effective radiative forcing time series (Fig. 2) are taken from Hansen et al. (2011). The aggregate of the forcing used for the model includes well-mixed greenhouse gases (WMGHGs)[9] including CO_2, stratospheric water vapour (Str. H_2O), stratospheric ozone (O_3), black carbon, stratospheric aerosols, snow albedo changes, land use changes, indirect aerosol effects and reflective aerosols. The short time period from 1955–2010 masks the dramatic increase in radiative forcing stemming from WMGHGs since the late 19th century. To estimate the parameters of the EBM here I rely on the aggregate of radiative forcing, an extension in Section 5.4.2 considers disaggregates by separating out volcanic forcing in the form of stratospheric aerosols.[10]

Among the three main IAMs: FUND, DICE, and PAGE, only DICE formally accounts for ocean–atmosphere interactions using a two-component calibrated energy balance model. Equally few econometric models accounting for non-stationarity in the form of stochastic trends also consider ocean heat content and thus the heat transfer between the atmosphere/top component and the ocean. Two notable exceptions are (Stern, 2006) using observations for ocean heat content up to 300 m depth, and Bruns et al. (2018) who consider a multi-cointegration approach reconstructing ocean heat content up to 2000 m for which few observations are available. Relative to these approaches I provide a direct link of the two-component EBM to a CVAR allowing for joint system estimation while using ocean heat content up to 700 m.

[8] Data for deeper ocean heat content for 0–2000 m is available but only through pentadal averages (Levitus et al., 2012).

[9] The major gases grouped together as WMGHGs include CO_2, CH_4, N_2O, and SF_6 (Sulphur hexafluoride) and are combined due to their long lifetime and property that they are "well-mixed" — concentrations are at approximately the same level across the globe (Myhre et al., 2013).

[10] Stern and Kaufmann (2014) test for links between individual forcing series and surface temperatures, further work could focus on more detailed models using individual forcing series found to be significant in Stern and Kaufmann (2014), while series with little impact (e.g. black carbon) could be omitted.

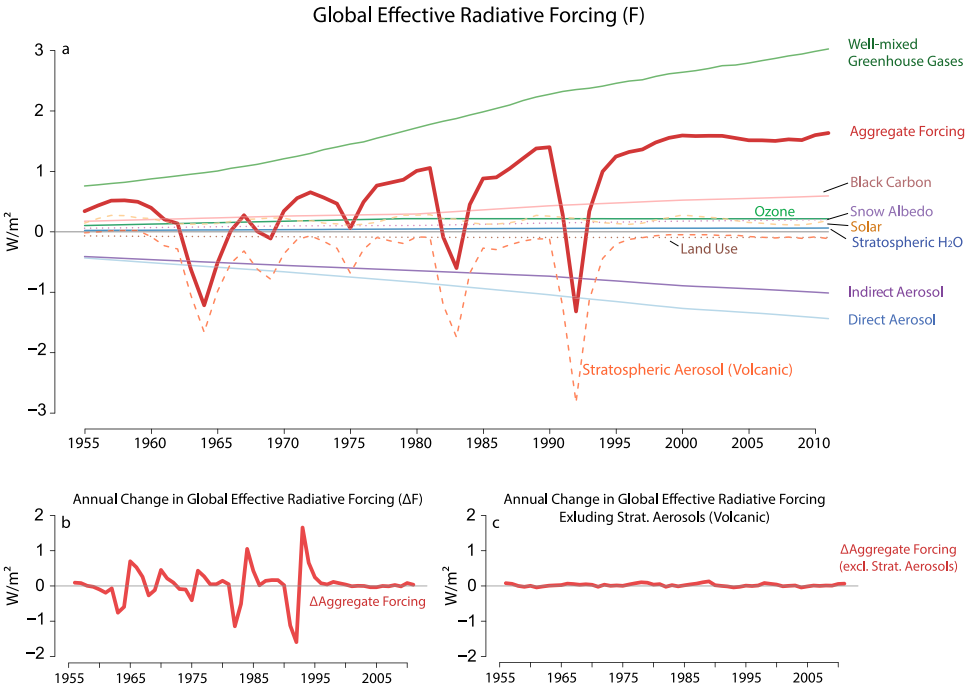

Fig. 2. Radiative forcing from 1955–2011 in W m^{-2}. Panel (a) shows global effective total and disaggregated forcing, panel (b) shows the first difference of total forcing, and panel (c) graphs first difference of total forcing excluding stratospheric aerosol forcing from volcanic eruptions.

Data availability for ocean heat content constrains the sample to a period from 1955 onwards. The estimation period is 1955–2011 at an annual frequency, resulting in T = 56 observations. This time period, together with the use of an aggregate of radiative forcing rather than individual series, alleviates some concerns over measurement changes and the data quality of the radiative forcing series (see Pretis and Hendry 2013).

While the time series properties of radiative forcing series are heavily debated within the climate-econometric literature (Kaufmann and Stern, 2002; Stern and Kaufmann, 2000; Beenstock et al., 2012; Pretis and Hendry, 2013), the individual order of integration of these series is not directly relevant. Within the EBM formulation it is aggregate forcing that drives upper component temperatures. On initial inspection it may appear inconsistent that global mean surface temperatures are well approximated by an I(1) process while well-mixed greenhouse gases and atmospheric CO_2 concentrations in particular can be argued to be I(2) — see supplementary material. However, jointly the individual forcing series sum (or cointegrate) to an I(1) aggregate of forcing, where the I(1) cointegrating relation is given simply by the sum of the individual forcing series. Given the same unit of measurement (watts per square metre), forcings are directly summable — this is a concern in the analysis of Beenstock et al. (2012) who argue that, due to the different time series properties, temperatures and WMGHGs cannot be related. Instead, while individual forcing series may be I(2) or I(0), aggregate forcing appears to be consistent with an I(1) process, and thus exhibits the same order of integration as global mean surface temperatures.

5.2. Estimation using ocean heat content observations

The EBM characterises changes in temperatures while the data available for applications often are a mixture of heat content and temperature observations. Given the availability of data, the present application uses ocean heat content (O_t) for the lower component and temperatures for the upper component. This transformation yields a re-parametrised, but otherwise identical EBM for estimation where I use $O_t \approx C_d T_{d,t}$ (see Schwartz, 2007 and Stern, 2006). The re-parametrised EBM is given as:

$$\begin{pmatrix} \Delta T_{m,t} \\ \Delta O_{,t} \\ \Delta F_t \end{pmatrix} = \begin{pmatrix} \tilde{\alpha}_{1,1} \\ \tilde{\alpha}_{2,1} \\ 0 \end{pmatrix} \begin{pmatrix} -\lambda & 0 & 1 \end{pmatrix} \begin{pmatrix} T_{m,t-1} \\ O_{t-1} \\ F_{t-1} \end{pmatrix} + \begin{pmatrix} \tilde{\alpha}_{1,2} \\ \tilde{\alpha}_{2,2} \\ 0 \end{pmatrix} \begin{pmatrix} 1 & -1/C_d & 0 \end{pmatrix} \begin{pmatrix} T_{m,t-1} \\ O_{t-1} \\ F_{t-1} \end{pmatrix} + \epsilon_t. \tag{20}$$

Let $\mathbf{h}_{1,t-1}$ and $\mathbf{h}_{2,t-1}$ in Eqs. (21) and (22) denote the two cointegrating vectors in the EBM–CVAR:

$$\mathbf{h}_{1,t-1} = \left(\beta_{1,1}T_{m,t-1} + \beta_{1,2}O_{t-1} + \beta_{1,3}F_{t-1}\right) \tag{21}$$

$$\mathbf{h}_{2,t-1} = \left(\beta_{2,1}T_{m,t-1} + \beta_{2,2}O_{t-1} + \beta_{2,3}F_{t-1}\right). \tag{22}$$

For identification both cointegrating vectors are normalised such that $\beta_{1,3} = 1$ and $\beta_{2,1} = 1$. The restrictions given by the EBM are: lower component temperatures do not enter the first cointegrating vector, $\beta_{1,2} = 0$; radiative forcing does not enter the second cointegrating vector, $\beta_{2,3} = 0$, and does not adjust to either cointegrating relationship ($\tilde{\alpha}_{3,1} = \tilde{\alpha}_{3,2} = 0$). This is a simplification since some of the radiative forcing series are potentially determined endogenously, CO_2 concentrations generally vary with temperatures, as does ice-albedo. However, it is not obvious whether this feedback is measurable and statistically significant on a global scale – Section 5.5.3 investigates the presence of feedback further.

To estimate the EBM model parameters of interest, the second cointegrating vector (22) provides an estimate of the heat capacity of the deep component using $\beta_{2,2} = -1/C_d$,. The climate feedback parameter λ can be determined using $\beta_{1,1} = -\lambda$. Approximate standard errors and confidence intervals can be derived using the asymptotic mixed normality of the cointegrating parameters. In the case of parameters of interest being non-linear transformations of the cointegrating estimates (such as $-1/C_d = \beta_{2,2}$), I rely on the δ-method to provide approximate standard errors of the estimates.[11]

5.3. Model specification

Determining the number of cointegrating relations and conducting inference on the estimated parameters relies on well-specified – congruent – models (Juselius, 2006). While the theoretical EBM model does not imply additional lags, the time series properties of the data may support a longer lag length. The estimated CVAR allowing for longer lags is provided here in Eq. (23):

$$\Delta\mathbf{Y}_t = \Gamma_1\Delta\mathbf{Y}_{t-1} + \cdots + \Gamma_k\Delta\mathbf{Y}_{t-k} + \mathbf{P}\mathbf{Y}_{t-1} + \Phi + \epsilon_t \tag{23}$$

where $\mathbf{Y}_t = (T_{m,t}, O_t, F_t)'$ and Φ denotes an unrestricted constant. To formally determine the lag structure I estimate a general unrestricted VAR (as in Eq. (14)) starting with three lags (equivalent to $k = 2$ in (23)). Removing the third lag is not rejected ($p = 0.08$), while dropping both the second and third lag is rejected ($p = 0.003$). The model with the lowest Schwarz criterion (SC, Schwarz, 1978) includes just one lag (SC = 3.28, relative to 3.45 for two, and 3.76 for three lags). Assessing the diagnostic tests of the unrestricted models, a VAR(1) model rejects no-residual autocorrelation (p = 0.003), while a VAR(2) passes the residual vector autocorrelation test (p = 0.59) and dropping the second lag in the VAR(2) is rejected (p = 0.005). Many discrete approximations use the average of two periods which further provides a justification for the use of two lags. Additional results on the dynamic stability and unit-root properties of the estimated VAR models are provided in the supplementary material.

I proceed by estimating three initial variants of the CVAR EBM model, referred to as models A, B, and C. First, model A is estimated with a single lag corresponding to the simple theory-based two-component EBM for comparison. Second, model B includes two lags as suggested by the tests determining the lag structure. Once the restrictions implied by the EBM are imposed, both models A and B do not model forcing explicitly but assume it to be weakly exogenous for the cointegrating relations. However, some of the forcing series may not be truly exogenous but rather vary with observed temperatures through natural (e.g. snow-albedo changes) and anthropogenic channels. Particularly, on a disaggregated level there is evidence that climate variability affects economic growth which subsequently may affect GHG emissions (Dell et al., 2014; Hsiang, 2016, with feedback discussed in Pretis, 2017). Therefore, Model C (estimated with 2 lags) relaxes the restrictions by allowing aggregate forcing to adjust to the first cointegrating relation ($\tilde{\alpha}_{3,1} \neq 0$). Section 5.5.3 investigates the presence of feedback on a global scale further. Volcanic forcing likely distorts inference in the base models A–C, subsequently Section 5.4.2 considers a model specification modelling volcanic eruptions as breaks (denoted as model V for volcanoes).

5.4. Results

The time series of global mean surface temperature anomalies, 0–700 m ocean heat content anomalies, and total radiative forcing cointegrate to two stationary relations consistent with the theory of a two-component EBM. Likelihood ratio tests do not reject the presence of two cointegrating vectors (rank = 2) in all base models (see Table 1). To address concerns about small samples, I also apply the bootstrap cointegration approach proposed by Cavaliere et al. (2012), as well as the Bartlett correction (Johansen, 2000), both of which confirm the results of the standard cointegration tests (Table 1).

[11] Given an asymptotically normally distributed random variable X satisfying $\sqrt{n}(X-\mu) \xrightarrow{D} N\left(0,\sigma^2\right)$ and a continuous function $g(\mu)$, using a Taylor-expansion we can approximate the distribution of $g(X)$ by $\sqrt{n}\left(g(X)-g(\mu)\right) \xrightarrow{D} N\left(0,\sigma^2[g'(\mu)]^2\right)$. However, if likelihood-ratio tests are being used, then linearisation is not required.

Table 1
Cointegration tests of the two-component EBM.

	A: Base, 1-lag	B & C: 2-lag	B & C: 2-lag bartlett	B & C: 2-lag bootstrap
Rank = 0	61.52 [p < 0.00]**	57.90 [p < 0.00]**	54.36 [p < 0.00]**	57.90 {cr5% = 41.28} [p < 0.00]**
Rank = 1	20.35 [p < 0.01]**	22.46 [p < 0.01]**	21.69 [p < 0.01]**	22.46 {cr5% = 20.56} [p = 0.01]**
Rank = 2	0.31 [p = 0.58]	0.09 [p = 0.76]	0.09 [p = 0.76]	0.09 {cr5% = 7.54} [p = 0.87]
Rank = 3	–	–	–	–
Obs.	56	55	55	55 ($B = 399$ Reps.)

Cointegration rank tests using the Johansen (1988) trace test, the Johansen trace test with Bartlett correction (Johansen, 2000), and bootstrap cointegration test (Cavaliere et al., 2012) with $B = 399$ bootstrap replications and reported 5% critical value as '{cr5% = ...}'. p-values are reported in brackets [ ], * indicates rejection at 5%, ** indicates rejection at 1%. Bartlett (and Bootstrap) results for Model A also support rank = 2 with p-values for rank = 2 of $p = 0.577$ ($p = 0.81$ for bootstr.) vs. $p < 0.01$ ($p = 0.028$ for bootstr.) for rank 1.

5.4.1. Model restrictions and diagnostics

Following tests on the rank (Table 1), I impose the reduced rank of two and estimate the CVAR models under the EBM restrictions from Section 5.2. Diagnostic test results for the presence of residual autocorrelation and normality are reported in Table 2, together with bootstrap and likelihood ratio tests of the EBM restrictions. Mis-specification of Model A (1-lag) is apparent through the presence of residual autocorrelation. While model B (2-lags) improves diagnostic specification, the EBM restrictions appear rejected. Model C (2-lag, endogenous forcing), in-turn, suggests a failure of normality of the residuals. The rejection of normality in C likely stems from the forcing series as indicated by the single-equation diagnostic tests — normality is not rejected in all but the forcing series. This can be driven by the sudden volcanic forcing resembling structural breaks. To explore sources of mis-specification, particularly the impact of potential structural breaks due to volcanic forcing, I apply indicator saturation methods to identify specific time-periods of model failure in the following Section 5.4.2.

5.4.2. Stability and detection of breaks

Mis-specification and the stability of the EBM over time can be assessed through formal econometric methods for the detection of outlying observations and structural breaks. Breaks in time series can arise in many shapes and may occur at any point in time — distorting inference in-sample and resulting in forecast failure out-of-sample if not appropriately modelled. Here I use impulse and step-indicator-saturation (IIS — see Hendry et al., 2008, and SIS — see Castle et al., 2015) to identify periods of instability which can be indicative of model mis-specification.[12]

Indicator saturation adds a full set of impulse or step-functions at every point in time and removes all but significant ones using general-to-specific selection up to a specified target level of significance p_α. This formulates the detection of breaks as a model-selection problem, where selection takes place over a full set of break functions, a subset of which describe any underlying breaks. If there are truly no outlying observations or breaks, then despite the inclusion of a large candidate set of dummy variables, the distribution of variables not-selected over (i.e. EBM parameters) remains unaffected beyond small efficiency effects (the asymptotic theory of block-partitioning is derived in Johansen and Nielsen, 2009 and Johansen and Nielsen, 2016, see also Jiao and Pretis, 2017). To assess uncertainties around break timings in SIS, the approximate normal distribution of the error terms can be used to construct approximate confidence intervals around a detected break in indicator saturation (Hendry and Pretis, 2017).

Using IIS and SIS in Models B and C (selecting at $p_\alpha = 1\%$) identifies one outlying observation as an impulse in 1977, and two opposite signed step-shifts in 1982 (99% confidence interval on breakdate: ± 1 year) and 1983 (99% CI: ± 1 year) denoting a negative shock in the early 1980s (Fig. 3, blue).[13] This negative structural break in the model of 0–700 m OHC in 1982/1983 coincides with the volcanic eruption of "El Chichón", suggesting that the volcanic impact may not have been modelled appropriately.[14] Indeed, volcanic forcing appears to act more as temporary structural breaks than continuous series (see Pretis et al., 2016 and Schneider et al., 2017), and further may explain some of the residual auto-correlation. Volcanic forcing $\left(F_{t,\text{Volc.}}\right)$ closely resembles an impulse, where the first difference of volcanic forcing $\left(\Delta F_{t,\text{Volc.}}\right)$ appears similar to a transitory shock dummy e.g. $(\ldots, 0, 1, -1, 0, \ldots)$ — see Fig. 2 panel *b*. This break-like behaviour likely drives the rejection of normality in Model C. There are multiple different ways in which volcanic forcing can be modelled within the CVAR specification. The aggregate forcing series F_t could be disaggregated and separated into exogenous and endogenous forcing series, alternatively eruptions could be treated as transitory shocks. Here I follow the latter approach in a fourth model specification (reported as Model V) where volcanic aerosol forcing are specified as breaks to avoid concerns of estimating climate sensitivities based on volcanic forcing in general (see e.g Lindzen and Giannitsis, 1998). Treating volcanic eruptions as closely resembling transitory breaks, I re-estimate the CVAR EBM with 2-lags, where the

[12] The literature on the detection of structural breaks is vast and many alternatives are available — see Perron (2006).

[13] The specified level of significance implies an expected false-positive rate for IIS of $0.01 \times T = 0.01 \times 55 = 0.5$ indicators retained spuriously by chance. The break in 1982 is captured by a single impulse in Model C, where an additional outlier is also detected in 2003 coinciding with sudden increased OHC.

[14] The event also coincides with the 1982–1982 El Niño which may explain model failure during this period — inclusion of El Niño measures such as the Southern Oscillation Index may provide an alternative modelling approach.

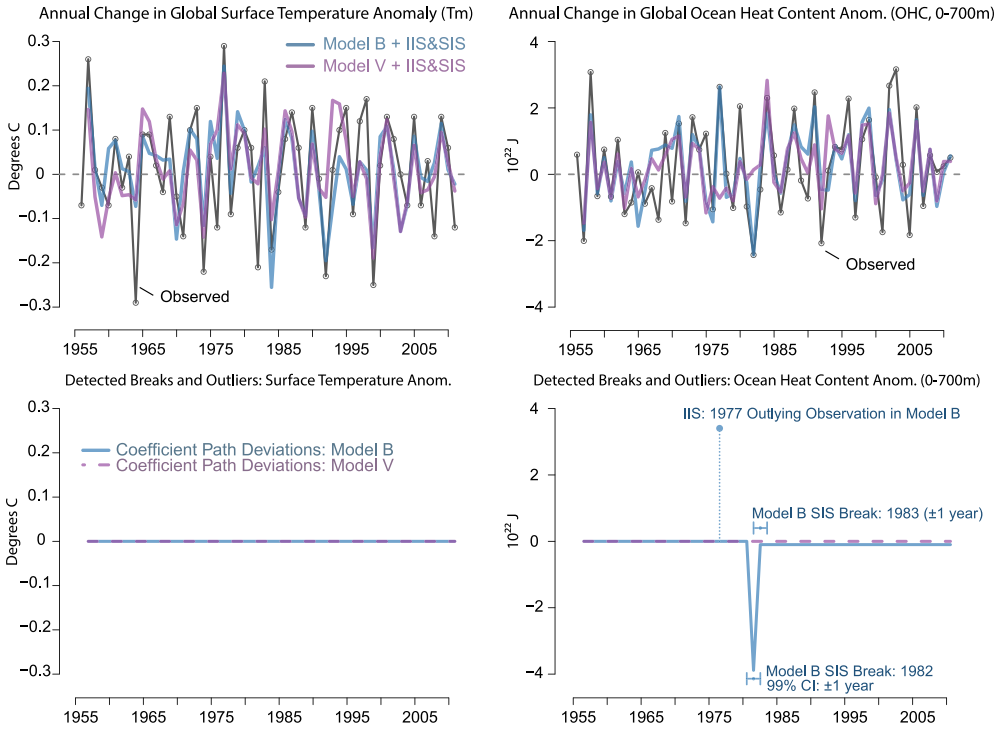

Fig. 3. Detected breaks using indicator saturation in model B (blue) and V (purple). Top: model fit using IIS and SIS. Bottom: deviations in the coefficient path — the time varying estimate of the intercept as determined using IIS and SIS, together with approximate dating uncertainty around detected step-shifts. (For interpretation of the references to colour in this figure legend, the reader is referred to the web version of this article.)

forcing series $\tilde{F}_t = F_t - F_{t,\text{Volc.}}$ enters the first cointegrating relation, and is itself restricted to be weakly exogenous for β.[15] The first difference of volcanic forcing, $\Delta F_{t,\text{Volc.}}$ enters the model unrestrictedly, similar to a transitory shock dummy.[16] The model now passes the diagnostic tests and the EBM restrictions are not rejected (see Table 2). Repeating the application of IIS and SIS for model V confirms that the improved model specification — when volcanic forcing is modelled as transitory breaks, no outliers or shifts are detected (see Fig. 3, purple).

5.4.3. Parameter estimates

Table 2 provides the estimated parameters of the CVAR for Models A (theory), B (2-lags), C (endogenous forcing), and V (volcanic breaks). Fitted values are shown in Fig. 4 for the first differences. Residual plots are provided in the supplementary material. The estimated parameters of the EBM in the cointegrating relations are highly significant and estimated with theory-consistent signs. Once the EBM-CVAR model satisfies the diagnostic tests, there is little evidence that the ocean heat content series adjusts to the first cointegrating vector ($\tilde{\alpha}_{2,1}$ is insignificant in Table 2).[17] This is consistent with the continuous-time EBM where the lower component only adjusts to the second cointegrating relation in (13).

5.5. Discussion

The CVAR specification places the econometric toolkit at the disposal of estimated EBMs. Here I consider the physical interpretation of the first cointegrating vector, the temperature response to increased forcing, the presence of feedback, and estimates of heat capacities.

5.5.1. Physical interpretation of first cointegrating vector

Based on the EBM in (1) and the equivalent cointegration formulation in (20), the first cointegrating relation used to estimate climate feedback λ, has a direct physical interpretation and describes the net heat flux or net energy coming into the system: $Q = F - \lambda T_m$. As an informal test of the model I compare the estimated cointegrating vector against

[15] The exact specification for Model V is: $\Delta \mathbf{Y}_t^* = \Gamma_1 \Delta \mathbf{Y}_{t-1}^* + \tilde{\alpha}\beta' \mathbf{Y}_{t-1}^* + \Phi + \theta \Delta F_{t,\text{volc}} + \epsilon_t$ where $\mathbf{Y}_t^* = \left(T_{m,t}, O_t, \tilde{F}_t\right)'$.

[16] The detected impulses are not included in the re-estimated model V.

[17] Further discussion of estimated model parameters is provided in the supplementary material.

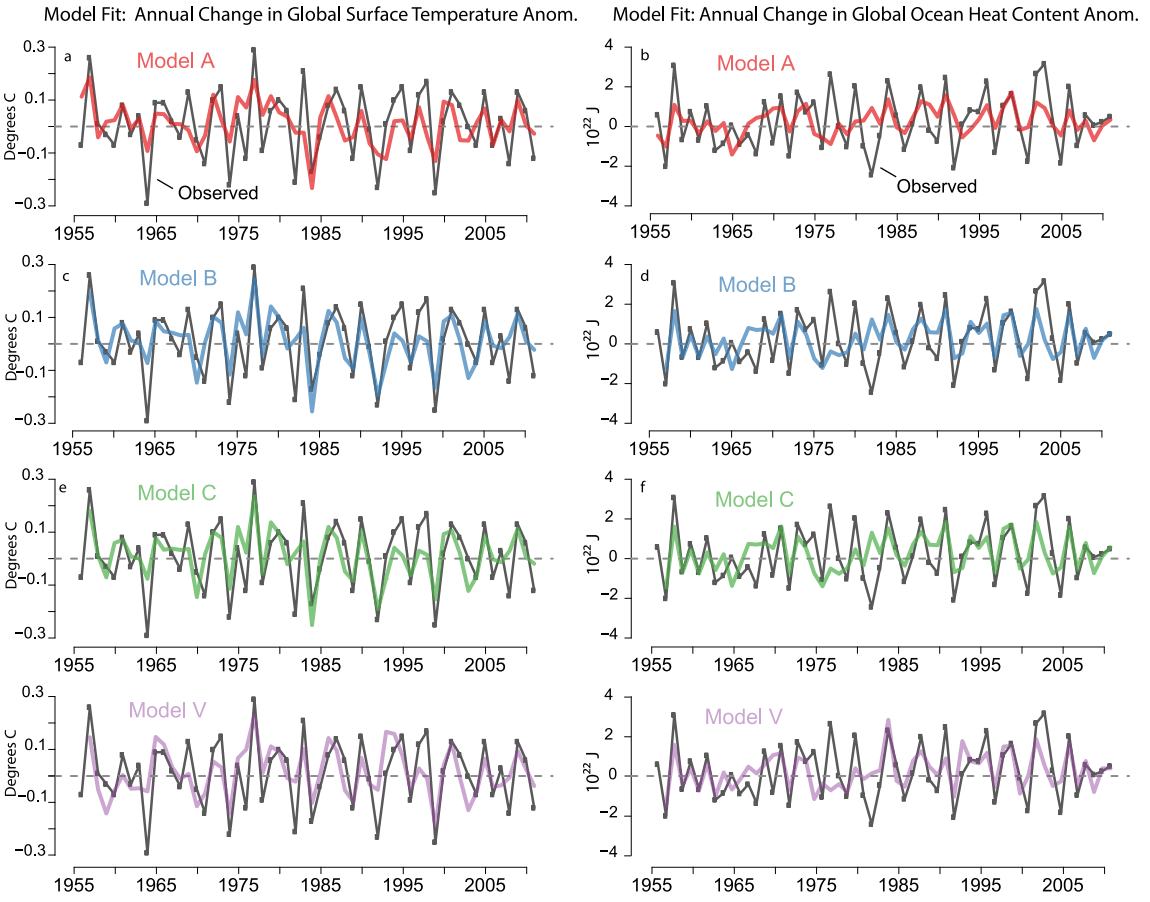

Fig. 4. EBM fit of first differences (estimated as a CVAR). Left panels show model fit (in colour) and observed first differences of (GIS) upper-component (global mean-surface) temperature anomalies (in black). Right panels show model fit and first differences of observed 0–700 m ocean heat content anomalies (Levitus et al., 2009) which proxy lower component heat content in the EBM. (For interpretation of the references to colour in this figure legend, the reader is referred to the web version of this article.)

the independently observed net flux from satellite-based measurements of annually averaged net flux at the top of the atmosphere (TOA) from the CERES Energy Balanced and Filled (EBAF) All Skies data (Loeb et al., 2009). It is important to emphasise that this data series is not used in the estimation of the model but is a different set of observations from satellite measurements of the quantity captured by the first cointegrating relation. Fig. 5 plots the first cointegrating relation together with the satellite measurements. The first cointegrating vector in all models matches the order of magnitude of the independent satellite observations. While the models under-estimate the level and variability slightly, the first cointegrating vector from model V remains close to the satellite-observed record. Model A, which does not control for residual autocorrelation and results in low estimates of climate sensitivity (see Section 5.5.2), consistently lies below satellite-observed TOA net flux.

5.5.2. Climate sensitivity and transient response

The system's response to an increase in emissions of GHGs is crucial for climate policy and assessment of future climate-related economic impacts. The estimates of the climate response to changes in emissions and thus concentrations of GHGs is characterised in the EBM by climate feedback λ and the estimated model dynamics.

Equilibrium climate sensitivity. A simple measure of the response of the system to increased forcing is given by the equilibrium climate sensitivity (ECS), defined as the equilibrium temperature response to the radiative forcing of a step-shift doubling of CO_2 concentrations.[18] Estimates of the ECS (see Table 2) depend on the model specification, where model mis-specification suggests an over-estimation of climate feedback λ and thus an under-estimation of the ECS.

[18] ECS for a doubling of CO_2 is derived from the steady-state equilibrium of the EBM. Using (4) and (5) in equilibrium it holds that $dT_m/dt = dT_d/dt = 0$ and thus $T_m = F/\lambda$. ECS is then defined as the equilibrium temperature response T_m given a radiative forcing of doubling of CO_2: ECS $= F_{2\times CO_2}/\lambda$, where $F_{2\times CO_2} \approx 3.7$ W m^{-2}.

Table 2
EBM Cointegration model parameter estimates where $\tilde{\alpha} = \alpha\kappa$.

	EBM/CVAR model			
Coint. relations	A: Base	B: 2-lag	C: Endo. Forc.	V: Volc. Breaks
Vector 1 (Mixed)				
$\beta_{1,1}$	−2.71 (0.51)**	2.29 (0.41)**	−2.21 (0.32)**	−1.71 (0.44)**
$\beta_{1,2}$	–	–	–	–
$\beta_{1,3}$	1	1	1	1
Adjustment				
$\tilde{\alpha}_{1,1}$	0.11 (0.03)**	0.15 (0.03)**	0.11 (0.03)**	0.21 (0.06)**
$\tilde{\alpha}_{1,2}$	0.60 (0.33)	0.53 (0.38)	−0.03 (0.41)	0.09 (0.81)
$\tilde{\alpha}_{1,3}$	–	–	−0.55 (0.15)**	–
Vector 2 (Deep)				
$\beta_{2,1}$	1	1	1	1
$\beta_{2,2}$	−0.044 (0.003)**	−0.041 (0.004)**	−0.041 (0.004)**	−0.042 (0.004)**
$\beta_{2,3}$	–	–	–	–
Adjustment				
$\tilde{\alpha}_{2,1}$	−0.41 (0.12)**	−0.46 (0.15)**	−0.47 (0.15)**	−0.65 (0.17)**
$\tilde{\alpha}_{2,2}$	7.82 (1.48)**	7.43 (1.99)**	7.35 (1.99)**	6.43 (2.04)**
$\tilde{\alpha}_{2,3}$	–	–	–	–
Test of Restric.				
$\chi^2(2)$, C: $\chi^2(1)$	12.87 [p = 0.012]*	16.32 [p = 0.003]**	2.47 [p = 0.12]	5.09 [p = 0.08]
Boostrap (B = 199)	cr5% = 10.8 [p = 0.07]	cr5% = 7.7 [p<0.01]**	cr5% = 3.7 [p = 0.12]	cr5% = 10.2 [p = 0.28]
Diagnostic tests				
AR (1-2) F-Test	2.96 [p = 0.005]**	1.32 [p = 0.24]	1.14 [p = 0.32]	1.37 [p = 0.21]
Normality χ^2	0.76 [p = 0.94]	7.19 [p = 0.13]	20.36 [p = 0.002]**	5.75 [p = 0.22]
Observations T	56	55	55	55
log-likelihood	−72.48	−59.85	−51.84	84.11
EBM estimates				
λ ($Wm^{-2}K^{-1}$)	2.71 (0.51)	2.29 (0.41)	2.21 (0.32)	1.71 (0.44)
ECS (C)	1.37 (0.25)[a]	1.62 (0.29)[a]	1.67 (0.24)[a]	2.16 (0.56)[a]
C_m (W year m^{-2} K^{-1})	–	–	–	–
C_d (W year m^{-2} K^{-1})	22.72 (1.54)[a]	24.39 (2.38)[a]	24.39 (2.38)[a]	23.8 (2.26)[a]
γ	–	–	–	–

Model estimates based on CVAR estimation. Standard errors are given in parentheses ( ) while p-values are reported in brackets [ ]. Bootstrap test for restrictions (Cavaliere et al., 2015) with B replications, 5% bootstrap critical values reported as '{cr5% = ...}'. Standard errors are provided where available. If no standard errors are reported, then parameter is restricted or derived from estimated model parameters. * indicates significance at 5%, ** indicates significance at 1%. Left column specifies parameters, right columns show estimation results. Dash marks imposed restriction and no identification in the case of the structural EBM parameters given the theoretical result of $\tilde{\alpha} = \alpha\kappa$.
[a]Standard errors derived using δ-method.

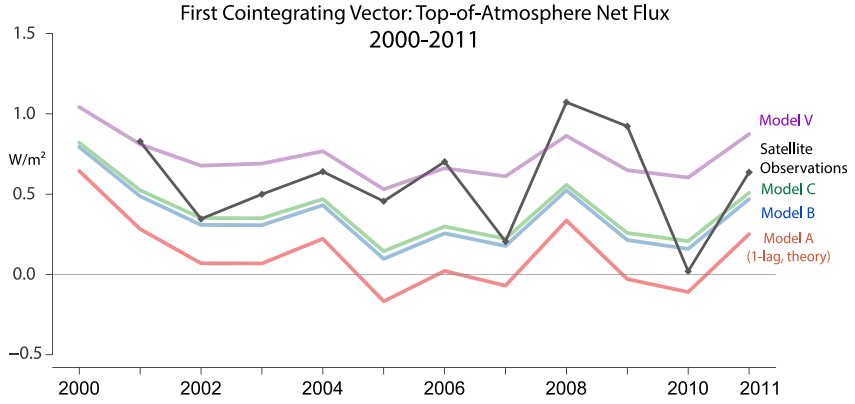

Fig. 5. Physical interpretation of the first cointegrating vector: Net flux based on the first cointegrating vector (Models A-V, colour) and observed top of the atmosphere (TOA) net flux 2000–2011. Annually averaged observed TOA net flux from the CERES Energy Balanced and Filled (EBAF) all skies data (black line with points) (Loeb et al., 2009) which have not been used to estimate the model and serve as an informal test of the model against a different set of independently measured observations.

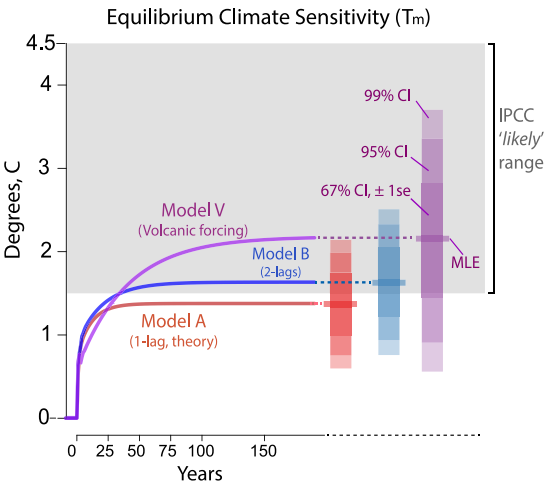

Fig. 6. Impulse response and estimated equilibrium climate sensitivity (ECS) – the equilibrium temperature response for a doubling of CO_2 for models A (theory), B (2-lags), and C (2-lags & endogenous forcing). Model V models volcanic forcing as breaks. MLE marks the maximum likelihood estimate, and shading denotes approximate confidence intervals (CI) from 67% (± 1 standard error, darkest) to 99% (lightest). The IPCC "likely" range is shown as grey shading for ECS. (For interpretation of the references to colour in this figure legend, the reader is referred to the web version of this article.)

In the mis-specified model A, λ is estimated to be 2.71 (se = 0.51) W m^{-2} C^{-1}, implying an ECS of 1.37 °C (se = 0.25). This is notably lower than the IPCC (IPCC, 2013) 'likely range' of 1.5 °C to 3 °C. A possible reason for why ECS may have been under-estimated in observation-based approaches (for example Schwartz (2007) finds ECS to be approximately 1.1 °C) can be model mis-specification (e.g apparent through residual autocorrelation and un-modelled breaks). Model V makes an attempt in correcting for this by treating volcanic forcing as transitory breaks. The climate feedback estimate in model V is notably lower than in models A-C, resulting in a higher estimate of ECS at 2.16 °C (se = 0.56). The estimate of ECS in model V is also associated with higher uncertainty (see Fig. 6, model V, purple) with a 95% confidence interval of 1.1 °C to 3.25 °C. To assess the time needed to reach equilibrium, Fig. 6 plots the impulse response functions of $T_{m,t}$ to a step-shift doubling of CO_2 concentrations.[19] In model V, half of the temperature response in the upper component is reached 17 years after the pulse (with 90% of the change after 80 years), while half of the change in OHC (the slower component) is reached after 29 years (with 90% reached after around 100 years).

Recursive estimation of ECS. To assess the stability of the estimated parameters over time I recursively estimate the model starting with a base sample of 20 observations from 1955–1976 onwards, expanding the sample up until 2011. This permits an assessment of whether the recent slowdown in increase in surface temperatures despite an increase in GHG concentrations (the "warming hiatus") affects the estimates of the model parameters. Fig. 7 graphs the recursively estimated ECS. Consistent with the findings of Otto et al. (2013) (who use a single component EBM), the point-estimates of ECS and climate feedback are relatively stable over the sample. Sudden increased ocean-heat uptake (see Fig. 1) likely drives higher uncertainty in 2003.[20] Overall, the inclusion of the hiatus period suggests stable point-estimates of ECS with higher uncertainties relative to the 1980s and 1990s.

Transient climate response. An alternative measure of the climate system's response to a change in forcing is the transient climate response (TCR) which describes the temperature change at the time of doubling CO_2 concentrations when concentrations are increased at the rate of 1% per year (see e.g. Otto et al., 2013). While the ECS can be inferred directly from the first cointegrating vector in the CVAR EBM, the TCR also depends on the short-run dynamic structure of the model. Here I report the estimates[21] of the TCR for the CVAR EBM when forcing is weakly (does not adjust to the cointegrating vectors) and strongly exogenous (no feedback), the unrestricted constant is dropped (it is insignificant in the equilibrium correction model), and short-run forcing variables only enter the upper-component temperature equation. The TCR estimates[22] are given by: 1.24 °C for model A, 1.38 °C for model B, and 1.38 °C for model V. To compare the CVAR

[19] Model C is omitted from the impulse–response analysis as it models forcing endogenously.

[20] The wide range of the $\pm$ 2 standard error interval for ECS in Fig. 7 primarily stems from the non-linear transformation of the climate feedback estimate $\hat{\lambda}$. The estimate for λ in model V falls close to zero in 2001–2003 leading to very high values (and uncertainty) of ECS which is a non-linear transformation of λ.

[21] Computed here for a 1% annual increase in CO_2 concentrations which implies a linear increase in forcing up until the time of doubling at a value of 3.71 W m^{-2}.

[22] Model C endogenizes forcing and so cannot be directly used to condition on a prescribed forcing path to compute TCR due to the presence of feedback.

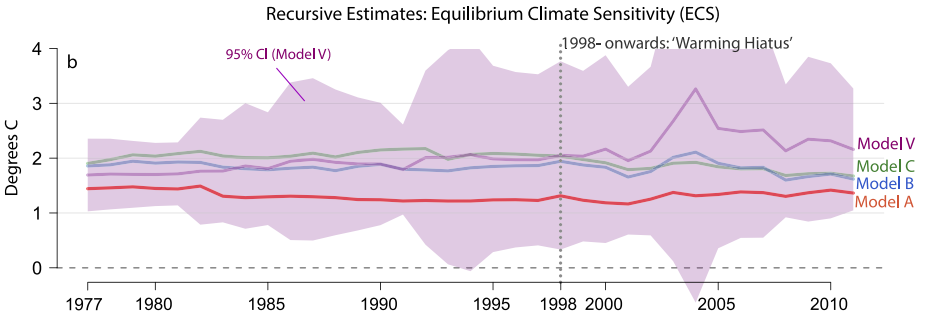

Fig. 7. Recursive Estimates of Equilibrium Climate Sensitivity (ECS). Figure shows the recursively estimated ECS for a radiative forcing of 3.7 W m^{-2} for a doubling of CO_2 with a base sample from 1956–1976 extended up to 1956–2011 for models A, B, C, and V. Purple shading denotes the approximate 95% confidence interval for model V. Standard errors for ECS are derived using the δ-method.

estimates of the TCR to those of Otto et al. (2013), I repeat the above analysis for a radiative forcing value for doubling of CO_2 of 3.44 W m^{-2}. This yields TCR estimates of 1.15 °C (Model A), 1.28 °C (Model B), and 1.28 °C (Model V), close to the preferred estimate of Otto et al. (2013) of around 1.3 °C.

5.5.3. Feedback onto radiative forcing

Temperatures respond to changes in radiative forcing, equally, radiative forcing may itself be affected by changes in temperatures. This feedback can stem from climate affecting human activity (through effects on productivity, land-use change, or economic growth — see Carleton and Hsiang, 2016), as well as natural channels such as temperatures effects on snow albedo and the natural uptake of GHGs. The EBM–CVAR specification makes it possible to test whether the feedback from temperatures (and ocean-heat) onto radiative forcing is measurable on a global scale. To assess the presence of feedback I disaggregate forcing F_t in model V into natural forcing known to be exogenous (solar and volcanic) and forcing potentially subject to feedback.[23] Subsequently, I re-estimate the model and test whether forcing adjusts to the equilibrium relationship (testing weak-exogeneity) and whether there is evidence of short-run feedback (testing strong-exogeneity).

There is little evidence that forcing measurably adjusts to the long-run equilibrium relationships. A joint test of excluding both cointegrating vectors from the forcing equation does not reject the restriction ($\chi^2 = 5.96$, [$p = 0.20$]; bootstrap [$p = 0.52$]). However, there is evidence of short-run feedback. The lagged first differences of temperatures and ocean-heat content cannot be excluded from the forcing equation (joint-test of excluding $\Delta T_{m,t-1}$ and ΔO_{t-1}: $\chi^2(2) = 12.21$, [$p = 0.002$]; individual tests ΔO_{t-1} : [$p = 0.02$], and $\Delta T_{m,t-1}$: [$p = 0.01$]). The exact channel of this feedback is difficult to determine on a global scale. It is likely that the measurable feedback is a combination of both a natural response of forcing to climate (such as reduced ocean CO_2 uptake with higher temperatures and changes in snow albedo), as well as anthropogenic responses to climate (such as changes in economic output and emissions with varying temperatures).

Weak-exogeneity of forcing for the cointegrating parameters means that inference on the equilibrium relationship between forcing and temperatures can be conducted without modelling the process of forcing itself. However, the absence of strong-exogeneity due to the presence of short-run feedback means there are concerns about the accuracy of climate forecasts conditional on forcing (e.g. using concentration scenarios) in the short-run.

5.5.4. Heat capacity estimates

The range of economic climate-damage projections due to uncertainties on physical parameters beyond the climate sensitivity in EBMs are not normally considered in IAMs (Calel and Stainforth, 2016).[24] The EBM-CVAR approach provides a way to jointly estimate climate sensitivity and heat capacities entering the models used to project economic damages.

The lower component heat capacity C_d can be estimated using $\beta_{2,2} = -1/C_d$. Estimates of the heat capacity of the lower component using the two-component EBM CVAR from model V suggests an effective ocean 0–700 m heat capacity of 23.8 (se = 2.26) W year m^{-2} C^{-1} (right panel in Fig. 8). This system-based estimate is higher than found by Schwartz (2012), who estimates the heat capacity of the lower component to be 14.1 W year m^{-2} C^{-1} using simple OLS regression. We may still under-estimate the total effective heat capacity of the system, mostly due to omission of the deeper ocean (>700 m). Equally, other heat sinks are omitted in this simple model. However, the response of OHC in the EBM CVAR

[23] The exact specification for the modified Model V to test feedback is: $\Delta \mathbf{Y}_t^{\dagger} = \Gamma_1 \Delta \mathbf{Y}_{t-1}^{\dagger} + \tilde{\alpha}\beta' \mathbf{Y}_{t-1}^{\dagger} + \Phi + \theta \Delta F_{t,\text{volc}} + \epsilon_t$ where $\mathbf{Y}_t^{\dagger} = \left(T_{m,t}, O_t, \breve{F}_t, F_{t,\text{solar}}\right)'$ and $\breve{F}_t = F_t - (F_{t,\text{solar}} + F_{t,\text{volc}})$.

[24] Nordhaus (2016) considers uncertainties on parameters in the carbon cycle of the DICE model as well as the ECS, however, does not examine the impact of uncertainties on heat capacity in the underlying EBM.

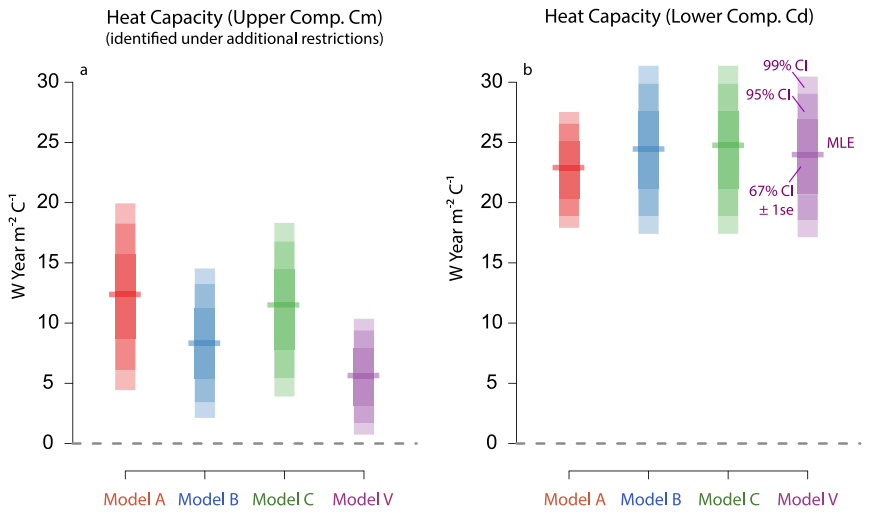

Fig. 8. Estimated heat capacities for Models A,B,C, and V. Left panel (a) shows the estimated heat capacity of the upper (mixed) component C_m which is identified when additional restrictions from Section 4.1.2 are imposed. Right panel (b) shows the estimates of the heat capacity of the deep component C_d without additional restrictions on adjustment coefficients. MLE marks the maximum likelihood estimate, and shading denotes approximate confidence intervals (CI) from 67% (± 1 standard error, darkest) to 99% (lightest).

to an increase in forcing is consistent with the findings of Joos et al. (2013) in orders of magnitude (see supplementary material for an impulse response).

To assess the dependence between estimates of heat capacity C_d and climate feedback λ as well as the ECS, I bootstrap the CVAR model and generate a sample of the cointegrating vectors. I find a negative relationship between parameter estimates of the heat capacity of the lower component C_d and climate feedback λ (see supplementary material). The quantified relationship between parameter estimates can help alleviate arbitrarily imposed covariances in EBMs in IAMs (Calel and Stainforth, 2016).

There is no one-to-one mapping between upper-component heat capacity C_m (the amount of energy needed to change the temperature T_m) and parameters in the exact Ornstein–Uhlenbeck CVAR representation of the continuous-time EBM. However, estimates of C_m can be obtained when imposing additional restrictions using the discrete-time approximation (Section 4.1.2). These are shown in Fig. 8 (left panel) and supplementary Table 4. Overall, the estimates of C_m and C_d show high uncertainties around component heat capacities (Fig. 8): a 95% confidence interval from model V suggests that the true value of C_d falls within a range of $\pm 20\%$ the point estimate, and $\pm 50\%$ for the point estimate of C_m. The uncertainties on heat capacities affect the time it takes the system to reach any new equilibrium temperatures following a change in forcing. In response to a step-shift doubling of CO_2, the lower (upper) range of heat capacity estimates implies that the equilibrium temperature could be reached approximately 10 years sooner (later) relative to the maximum likelihood estimates.

6. Conclusion

I showed how econometric system models of climate can be estimated in ways consistent with the underlying physics. Doing so, I provide a basis for empirical models of climate-economic systems, which are vital to correctly assess the economic costs of climate change. Formally, I demonstrated the mathematical equivalence of a two-component energy balance model (EBM) to a cointegrated system that can be mapped to a cointegrated vector autoregression (CVAR) in discrete time. The equivalence provides a physical basis for the use of econometric CVARs in climate-economic research, placing the entire toolkit of CVARs at the disposal of energy balance models. The resulting system-based estimation can be used to quantify parameter uncertainties in projections of the economic damages from climate change in integrated assessment models.

In an application, I estimated a two-component EBM using global mean surface temperature anomalies, 0–700 m ocean heat content anomalies, and aggregates of radiative forcing showed the model not to be rejected. Standard and bootstrap cointegration tests confirmed that the time series form two stationary relations and cointegrate in ways consistent with theory. Individual parameters were statistically significant with theory-consistent signs and independent satellite observations closely tracked the estimates of the first cointegrating vector. CVAR estimation of a two-component EBM showed that point estimates of the temperature responses to increased forcing (e.g., from CO_2 concentrations) were relatively stable over the sample of observations, although, the recent slowdown in warming is associated with higher parameter uncertainties. I found that model mis-specification (apparent through residual autocorrelation) results in high values of the observationally-determined climate feedback, and in turn, may lead to an under-estimation of

the equilibrium climate sensitivity. By improving model specification through the detection and modelling of structural breaks, I showed that uncertainties on key parameters beyond climate sensitivity (such as heat capacities) are high and need to be accounted for in economic impact projections.

This paper provides a foundation for the use of CVARs – which are commonly used to model the macroeconomy – in estimating climate econometric systems consistent with physical laws. This allows socio-economic models to be linked to climate models by estimating a system where the forcing series are endogenized and driven by economic activity. More generally, this enables the coupling of empirical climate models with empirical macroeconomic systems to address concerns with existing climate-economic models (Burke et al., 2016; Pindyck, 2013; Stern, 2013, 2016). Furthermore, using econometric methods to identify shifts in models (Castle et al., 2015; Estrada et al., 2013; Pretis and Allen, 2013) allows an assessment of the impacts of policy effectiveness and natural shocks. A system model that is consistent with physical laws also permits the feedback of climate variables into the economy to be estimated, opening the door to data-driven system models of interactions between the economy and climate.

Acknowledgements

Financial support from the Oxford Martin School, UK, Open Society Foundations, United States, Robertson Foundation, United States, and British Academy, UK is gratefully acknowledged. I thank two anonymous reviewers for helpful comments. I am grateful to Janine Aron, John Fyfe, Niels Haldrup, James Hamilton, David F. Hendry, Eric Hillebrand, Ole Jann, Søren Johansen, Katarina Juselius, Robert K. Kaufmann, Andrew B. Martinez, Bent Nielsen, Heino Bohn Nielsen, Peter C.B. Phillips, Bary Pradelski, Tommaso Proietti, Anders Rahbek, David Ronayne, and Max Roser for comments and suggestions.

Appendix A. Supplementary material

Supplementary material related to this article can be found online at https://doi.org/10.1016/j.jeconom.2019.05.013.

References

Beenstock, M., Reingewertz, Y., Paldor, N., 2012. Polynomial cointegration tests of anthropogenic impact on global warming. Earth Syst. Dyn. 3 (2), 173–188.

Bruns, B., Stephan, Csereklyei, Z., Stern, I., David, 2018. A multicointegration model of global climate change. Working Paper, http://dx.doi.org/10.2139/ssrn.3117015.

Burke, M., Craxton, M., Kolstad, C., Onda, C., Allcott, H., Baker, E. …, et al., 2016. Opportunities for advances in climate change economics. Science 352 (6283), 292–293.

Burke, M., Hsiang, S.M., Miguel, E., 2015. Global non-linear effect of temperature on economic production. Nature 527 (7577), 235–239.

Calel, R., Stainforth, D.A., 2016. On the physics of three integrated assessment models. Bull. Amer. Meteorol. Soc. (89).

Carleton, T.A., Hsiang, S.M., 2016. Social and economic impacts of climate. Science 353 (6304).

Castle, J.L., Doornik, J.A., Hendry, D.F., Pretis, F., 2015. Detecting location shifts during model selection by step-indicator saturation. Econometrics 3 (2), 240–264.

Cavaliere, G., Nielsen, H.B., Rahbek, A., 2015. Bootstrap testing of hypotheses on co-integration relations in vector autoregressive models. Econometrica 83 (2), 813–831.

Cavaliere, G., Rahbek, A., Taylor, A., 2012. Bootstrap determination of the co-integration rank in vector autoregressive models. Econometrica 80 (4), 1721–1740.

Dell, M., Jones, B.F., Olken, B.A., 2012. Temperature shocks and economic growth: Evidence from the last half century. Amer. Econ. J.: Macroecon. 4 (3), 66–95.

Dell, M., Jones, B.F., Olken, B.A., 2014. What do we learn from the weather? The new climate–economy literature. J. Econ. Lit. 52 (3), 740–798.

Doornik, J.A., 2016. CATS in Ox. Timberlake Consultants, London.

Doornik, J.A., Hendry, D., 2013. PcGIve 14. Timberlake Consultants, London.

Engle, R.F., Granger, C.W.J., 1987. Co-integration and error correction: Representation, estimation, and testing. Econometrica 55 (2), 251–276.

Estrada, F., Gay, C., Sánchez, A., 2010. A reply to: 'Does temperature contain a stochastic trend? Evaluating conflicting statistical results' by RK Kaufmann et al. Clim. Change 101 (3), 407–414.

Estrada, F., Perron, P., 2014. Detection and attribution of climate change through econometric methods. Bol. Soc. Mat. Mexicana 20 (1), 107–136.

Estrada, F., Perron, P., Martínez-López, B., 2013. Statistically derived contributions of diverse human influences to twentieth-century temperature changes. Nat. Geosci. 6, 1050–1055.

Gregory, J., Stouffer, R., Raper, S., Stott, P., Rayner, N., 2002. An observationally based estimate of the climate sensitivity. J. Clim. 15 (22), 3117–3121.

Hansen, J., Ruedy, R., Sato, M., Lo, K., 2010. Global surface temperature change. Rev. Geophys. 48 (4).

Hansen, J., Sato, M., Kharecha, P., Schuckmann, K.v., 2011. Earth's energy imbalance and implications. Atmospheric Chem. Phys. 11 (24), 13421–13449.

Held, I.M., Winton, M., Takahashi, K., Delworth, T., Zeng, F., Vallis, G.K., 2010. Probing the fast and slow components of global warming by returning abruptly to preindustrial forcing. J. Clim. 23 (9), 2418–2427.

Hendry, D.F., Johansen, S., Santos, C., 2008. Automatic selection of indicators in a fully saturated regression. Comput. Stat. 23, 337–339.

Hendry, D.F., Pretis, F., 2013. Anthropogenic influences on atmospheric CO2. Handb. Energy Clim. Change 287.

Hendry, D.F., Pretis, F., 2017. Quantifying the uncertainty around break dates in step-indicator saturation. Oxford Economics Working Paper.

Hope, C., 2011. The social cost of CO2 from the PAGE09 model. Discussion Paper.

Hope, C., Anderson, J., Wenman, P., 1993. Policy analysis of the greenhouse effect: an application of the PAGE model. Energy Policy 21 (3), 327–338.

Hsiang, S.M., 2016. Climate econometrics. Annu. Rev. Resour. Econ. 8, 43–75.

Hutzenthaler, M., Jentzen, A., Kloeden, P.E., 2011. Strong and weak divergence in finite time of euler's method for stochastic differential equations with non-globally lipschitz continuous coefficients. Proc. R. Soc. Lond. A 467, 1563–1576.

IPCC, 2013. Fith assessment report: Climate change 2013: Working Group I Report: The Physical Science Basis. Geneva: IPCC. https://www.ipcc.ch/report/ar5/wg1/.

Jiao, X., Pretis, F., 2017. Testing the presence of outliers to assess misspecification in regression models. Oxford Economics Working Paper.
Johansen, S., 1988. Statistical analysis of cointegration vectors. J. Econ. Dyn. Control 12, 231–254.
Johansen, S., 1995. Likelihood-Based Inference in Cointegrated Vector Autoregressive Models. Oxford University Press, Oxford.
Johansen, S., 2000. A bartlett correction factor for tests on the cointegrating relations. Econometric Theory 16 (05), 740–778.
Johansen, S., Nielsen, B., 2009. In: Castle, J.L., Shephard, N. (Eds.), An Analysis of the Indicator Saturation Estimator As a Robust Regression Estimator. Oxford University Press, Oxford, pp. 1–36.
Johansen, S., Nielsen, B., 2016. Asymptotic theory of outlier detection algorithms for linear time series regression models. Scand. J. Stat. 43 (2), 321–348.
Joos, F., Roth, R., Fuglestvedt, J., Peters, G., Enting, I., Bloh, W.v., et al., 2013. CaRbon dioxide and climate impulse response functions for the computation of greenhouse gas metrics: a multi-model analysis. Atmospheric Chem. Phys. 13 (5), 2793–2825.
Juselius, K., 2006. The Cointegrated VAR Model: Methodology and Applications. Oxford University Press, Oxford.
Juselius, K., 2011. Co-integration analysis of climate change: An exposition. Working Paper.
Kaufmann, R.K., Juselius, K., 2013. Testing hypotheses about glacial cycles against the observational record. Paleoceanography 28 (1), 175–184.
Kaufmann, R.K., Kauppi, H., Mann, M.L., Stock, J.H., 2011. Reconciling anthropogenic climate change with observed temperature 1998–2008. Proc. Natl. Acad. Sci. 108 (29), 11790–11793.
Kaufmann, R.K., Kauppi, H., Mann, M.L., Stock, J.H., 2013. Does temperature contain a stochastic trend: linking statistical results to physical mechanisms. Clim. change 1–15.
Kaufmann, R.K., Kauppi, H., Stock, J.H., 2010. Does temperature contain a stochastic trend? evaluating conflicting statistical results. Clim. change 101 (3–4), 395–405.
Kaufmann, R.K., Stern, D.I., 2002. Cointegration analysis of hemispheric temperature relations. J. Geophys. Res. 107 (2).
Kessler, M., Rahbek, A., 2001. Asymptotic likelihood based inference for co-integrated homogenous gaussian diffusions. Scand. J. Stat. 28 (3), 455–470.
Kessler, M., Rahbek, A., 2004. Identification and inference for multivariate cointegrated and ergodic gaussian diffusions. Stat. Inference Stoch. Process. 7 (2), 137–151.
Kloeden, P.E., Platen, E., 1992. Numerical Solution of Stochastic Differential Equations. Springer.
Levitus, S., Antonov, J., Boyer, T., Baranova, O., Garcia, H., Locarnini, R. ., et al., 2012. World ocean heat content and thermosteric sea level change (0–2000 m), 1955–2010. Geophys. Res. Lett. 39 (10).
Levitus, S., Antonov, J., Boyer, T., Locarnini, R., Garcia, H., Mishonov, A., 2009. Global ocean heat content 1955–2008 in light of recently revealed instrumentation problems. Geophys. Res. Lett. 36 (7).
Lindzen, R.S., Giannitsis, C., 1998. On the climatic implications of volcanic cooling. J. Geophys. Res.: Atmospheres (1984-2012) 103 (D6), 5929–5941.
Loeb, N.G., Wielicki, B.A., Doelling, D.R., Smith, G.L., Keyes, D.F., Kato, S. ., Wong, T., 2009. Toward optimal closure of the earth's top-of-atmosphere radiation budget. J. Clim. 22 (3).
Magnus, J.R., Melenberg, B., Muris, C., 2011. Global warming and local dimming: The statistical evidence. J. Amer. Statist. Assoc. 106 (494), 452–464.
Myhre, G., Shindell, D., Breon, F., Collins, W., Fuglestvedt, J., Huang, J., Zhang, H., 2013. Anthropogenic and natural radiative forcing climate change 2013: The physical science basis. In: Contribution of Working Group I To the Fifth Assessment Report of the Intergovernmental Panel on Climate Change. Cambridge University Press, Cambridge, UK.
Nielsen, B., 2006. Order Determination in General Vector Autoregressions. In: Time series and related topics, Institute of Mathematical Statistics, pp. 93–112.
Nordhaus, W., 2014. Estimates of the social cost of carbon: concepts and results from the DICE-2013r model and alternative approaches. J. Assoc. Environ. Resour. Econ. 1 (1/2), 273–312.
Nordhaus, W., 2016. Projections and Uncertainties About Climate Change in an Era of Minimal Climate Policies (Tech. Rep.). National Bureau of Economic Research.
Otto, A., Otto, F.E., Boucher, O., Church, J., Hegerl, G., Forster, P.M., et al., 2013. Energy budget constraints on climate response. Nat. Geosci. 6 (6), 415–416.
Perron, P., 2006. Dealing with structural breaks. Palgrave Handb. Econometrics 1, 278–352.
Phillips, P.C., 1991. Error correction and long-run equilibrium in continuous time. Econometrica 967–980.
Pindyck, R.S., 2013. Climate change policy: What do the models tell us?. J. Econ. Lit. 51 (3), 860–872.
Pretis, F., 2017. Exogeneity in climate econometrics. Oxford Economics Discussion Paper, Available at SSRN: https://ssrn.com//abstract=2898203.
Pretis, F., Allen, M., 2013. Climate science: Breaks in trends. Nat. Geosci. 6, 992–993.
Pretis, F., Hendry, D., 2013. Some hazards in econometric modelling of climate change. comment on 'polynomial cointegration tests of anthropogenic impact on global warming' by beenstock et al. (2012). Earth Syst. Dyn. 4 (2), 375–384.
Pretis, F., Reade, J., Sucarrat, G., 2018a. General-to-specific (GETS) modelling and indicator saturation with the r package gets. J. Statist. Softw. 86 (3).
Pretis, F., Schneider, L., Smerdon, J.E., Hendry, D.F., 2016. Detecting volcanic eruptions in temperature reconstructions by designed break-indicator saturation. J. Econ. Surv. http://dx.doi.org/10.1111/joes.12148.
Pretis, F., Schwarz, M., Tang, K., Haustein, K., Allen, M., 2018b. Uncertain impacts on economic growth when stabilizing global temperatures at 1.5c or 2c warming. Phil. Trans. R. Soc. A 376.
Sargan, J., 1974. Some discrete approximations to continuous time stochastic models. J. R. Stat. Soc. Ser. B 74–90.
Schmith, T., Johansen, S., Thejll, P., 2012. Statistical analysis of global surface temperature and sea level using cointegration methods. J. Clim. 25 (22), 7822–7833.
Schneider, L., Smerdon, J., Pretis, F., Hartl-Meier, C., Esper, J., 2017. A new archive of large volcanic events over the past millennium derived from reconstructed summer temperatures. Environ. Res. Lett. 12 (9).
Schwartz, S.E., 2007. Heat capacity, time constant, and sensitivity of earth's climate system. J. Geophys. Res. 112 (D24), D24S05.
Schwartz, S.E., 2012. Determination of earth's transient and equilibrium climate sensitivities from observations over the twentieth century: strong dependence on assumed forcing. Surv. Geophys. 33 (3–4), 745–777.
Schwarz, G., 1978. Estimating the dimension of a model. Ann. Statist. 6, 461–464.
Stern, I.D., 2006. An atmosphere–ocean time series model of global climate change. Comput. Stat. Data Anal. 51 (2), 1330–1346.
Stern, N., 2013. The structure of economic modeling of the potential impacts of climate change: grafting gross underestimation of risk onto already narrow science models. J. Econ. Lit. 51 (3), 838–859.
Stern, N., 2016. Economics: Current climate models are grossly misleading. Nature 530 (7591), 407–409.
Stern, D.I., Kaufmann, R.K., 2000. Detecting a global warming signal in hemispheric temperature series: A structural time series analysis. Clim. Change 47, 411–438.
Stern, D.I., Kaufmann, R.K., 2014. Anthropogenic and natural causes of climate change. Clim. Change 122 (1–2), 257–269.
Storelvmo, T., Leirvik, T., Lohmann, U., Phillips, P.C., Wild, M., 2016. Disentangling greenhouse warming and aerosol cooling to reveal earth's climate sensitivity. Nat. Geosci. 9 (4), 286–289.
Waldhoff, S.T., Anthoff, D., Rose, S., Tol, R.S., 2011. The marginal damage costs of different greenhouse gases: An application of FUND. Discussion Paper.